Desalination and Water Treatment
www.deswater.com

doi: 10.5004/dwt.2021.27503

231 (2021) 359–366
August

Removal of high-concentration sulfate ions from industrial wastewater using low-cost modified Jordanian kaolin

Banan Hudaib[a], Ali F. Al-Shawabkeh[b], Waid Omar[a,*], Habis Al-Zoubi[c], Rund Abu-Zurayk[d]

[a]*Chemical Engineering Department, Faculty of Engineering Technology, Al-Balqa Applied University, Amman 11134, Jordan, Tel. +962792818634; emails: waid.omar@bau.edu.jo (W. Omar), banan.hudaib@bau.edu.jo (B. Hudaib)*
[b]*Physics and Basic Sciences Department, Faculty of Engineering Technology, Al-Balqa Applied University, Amman 11134, Jordan, email: drshawabkeh@bau.edu.jo*
[c]*Department of Chemical Engineering, College of Engineering, Al-Hussein Bin Talal University, P.O. Box: 20, Ma'an, Jordan, email: habisal-zoubi@ahu.edu.jo*
[d]*Hamdi Mango Center for Scientific Research. HMCSR, University of Jordan, Amman 11942, Jordan, email: r.abuzurayk@ju.edu.jo*

Received 10 February 2021; Accepted 4 June 2021

ABSTRACT

This research investigates kaolin's adsorption potential from the Mahis area in Jordan as an adsorbent to treat wastewaters contaminated with a high concentration of sulfate ions in aqueous solutions. Artificial wastewater was studied of 500 mg/L sulfate ions concentration and at pH = 5.5. The kaolin used was modified by sorption of $BaCl_2$ on its surface. A fixed-bed column (particle size 4 mm; bed height 7 cm; bed mass 35 g) was used to measure breakthrough curves to evaluate sulfate ions' adsorption behavior onto the modified kaolin at different flow rates. For the studied flow rates of 6.6, 12, and 24 mL/min, the measured breakthrough times are 50, 24, and 13 min respectively, while the exhaust times are 75, 50, and 40 min respectively. The measured breakthrough curves are analyzed by the mathematical models: Bohart–Adams model, Thomas model and Yoon–Nelson model. The calculated maximum adsorption capacity from the Bohart–Adams model is 46,838.34 mg/L at a flow rate of 24 mL/min. Thomas rate constant values are nearly constant at 0.0001 L/min mg at all flow rates. The estimated values from the Yoon–Nelson model of the time needed to reach 50% of the breakthrough are 43.96, 20.88, and 13.46 min the flow rates 6.6, 12, and 24 mL/min, respectively. Yoon–Nelson model fits the measured breakthrough curve to a higher degree than the Bohart–Adams model.

Keywords: Adsorption; Breakthrough; Sulfate; Wastewater; Kaolin; Fixed-bed column

1. Introduction

Water security is a big concern for water-scarce countries facing changing water challenges due to deficient water supply, climate change, and increasing water demand [1]. Freshwater is essential to human health, and it affects ancillary activities needed for survival. Needed for freshwater is rising with many factors like population growth, the pollution of water, and technological progress. On a per-capita basis, Jordan has one of the world's lowest water resources [2]. Jordan has faced deficits in water resources early since the 1960s. It is sorted number ten in the world concerning the shortage in water [3]. In many industries such as aluminum productions, controlling the quantity and quality of water intake and water discharge has become critical due to freshwater resources and

* Corresponding author.

environmental issues [3]. Most of these industrial processes require a high amount of water use, which reveals the need to apply a cheap way to reuse this discharged water or use it, for example, for irrigations.

Sulfate ions (SO_4^{2-}) are found in many types of wastewaters worldwide, such as the wastewaters produced from the oxidation of sulfide minerals, steel mills, and sulfate-pulp mills, and textile plants [4]. In Jordan large quantities of wastewater contaminated with sulfate ions are discharged from the Phosphate Mines. The digestion process of phosphate rock for production of Single Super Phosphate involves acidification with sulfuric acid. The sulfate content of the wastewater at Al-Abyad EW phosphate mines reached 790.8 mg/L [5] and at Eshydia mines 386 mg/L [6]. Moreover, wastewaters produced from many local industries such as pharmaceutical factories, printing, and dyeing processes contribute in increasing the quantities of wastewaters contaminated with sulfate ions in Jordan.

Although SO_4^{2-} is a well-known and non-toxic component of many kinds of water bodies, high concentrations of SO_4^{2-} in the water can cause a significant environmental problem, such as water mineralization, metal corrosion, toxic hydrogen sulfide release, pipes scaling, and disruption in the balance of the natural sulfur cycle [7–10]. Also, high concentrations of SO_4^{2-} (>600 mg/L) in the water can cause taste and health issues such as laxative problems in mammals [2,11]. The maximum level of sulfate suggested by the World Health Organization (WHO) standards is 250 mg/L of sulfate in water intended for human consumption [12]. Many countries like Jordan set the industrial effluent range as (200–500 mg/L) [13]. Hence, developing useful, low-cost, and sustainable treatment methods for removing sulfate is a need to meet the industrial process demands (the recycling of desulfurization wastewater) and environmental regulation.

There are many conventional processes for removing high concentrations of sulfate ions from industrial wastewater streams, such as membrane filtration (nanofiltration membrane and reverse osmosis) [14,15], flotation process [16], chemical precipitation, coagulation, and ion exchange [17]. These processes have many drawbacks, such as high energy, high reagent costs, and notably toxic sludge disposal [16,18]. Adsorption methods, either batch or continuous columns, are becoming one of the most critical approaches due to their lower costs and higher efficiency [18–23]. Adsorption of sulfate on clay minerals is an effective chemical process controlling their migration in soil and aquifer; furthermore, the adsorptive properties of clay make it valuable as cost-effective material that can find practical application to prevent the migration of toxic ions into groundwater [16,24].

Many clay types have been studied for wastewater treatment, like, kaolinite [19,25] and montmorillonite [26] as a low-cost adsorbent due to its metal binding capacity. Kaolinite [$Al_2Si_2O_5(OH)_4$] is a common phyllosilicate mineral formed through geological processes decomposition of feldspars. Kaolin natural deposits are inexpensive and available richly in different locations in Jordan. These deposits are distributed throughout Jordan in the north (e.g., Jarash area), central (e.g., Mahis area), and in the south (e.g., Batn El-Ghoul, Al Mudawwara, Ghor Kabid, Jabel Umm Saham, and Dubaydib areas) [2]. Modification of kaolin clay methods has been studied around the world to enhance the surface properties of amorphized (grounded) kaolin through acid activation [27], mechanochemical activation [28], and clay composites [29].

In this work, the surface properties of kaolin will be modified by sorption of $BaCl_2$ on its surface [30]. Kaolin clay was obtained from the Mahis location in Jordan and investigated as a potential and low-cost adsorbent for high concentration sulfate ions in aqueous solutions. Continuous fixed-bed experiments were carried out to investigate the adsorption potential of sulfate ions on the treated kaolin adsorbent. The kinetic parameters of the Bohart–Adams model, Thomas model, and Yoon and Nelson model were determined.

2. Experimental part

2.1. Materials

All the experiments were conducted with artificial wastewater stock solution prepared by dissolving analytical grade Na_2SO_4 to distilled water. The stock solution was diluted to a specific concentration and stored at 25°C. Clay samples obtained from the Mahis area were used as adsorbent material.

Kaolin clay was collected from the Mahis area, Jordan. It was crushed and sieved to 5 and 10 mesh size. Then it was washed and mixed with NaCl solution (0.9 M) and stirred for 4 h. The excess NaCl was then washed and dried at 120°C for 20 min. After that, it was mixed with barium chloride solution (0.5 M) and stirred for 8 h. Finally, washed with ultrapure water and dried at 120°C for 20 min. The $BaCl_2$ is supposed to be adsorbed to the surface of the kaolin.

2.2. Characterization of kaolin

Both raw kaolin and modified kaolin were characterized using Fourier-transform infrared spectroscopy (FTIR) instrument, model PerkinElmer, Spectrum Two L1600400, FT-IR/DTGS. The chemical composition of raw kaolin without any treatment used in this study as the adsorbent was analyzed using ThermoFisher XRF Instrument, model ARL™ SMS-Omega.

2.3. Apparatus

Fig. 1 demonstrates the experimental apparatus used to measure the continuous adsorption of sulfate ions on kaolin. Breakthrough curves were measured by collecting effluent samples at regular periods and measuring each sample's time, volume, and concentration.

The prepared artificial sulfate contaminated wastewater solution was stored in a tightly sealed 20 L feed vessel. The initial concentration of sulfate ions was 500 mg/L, and its pH = 5.5. The adsorption column is a cylindrical glass tube with a cross-sectional area of 1.92 cm^2 and 40 cm length. The kaolin was packed inside the column until the desired bed height and mass is attained. The backed column was kept stable by fixing a fiberglass wool layer at the top and the bottom of the backing to prevent adsorbent loss with the flowing solution, thus ensuring a constant mass

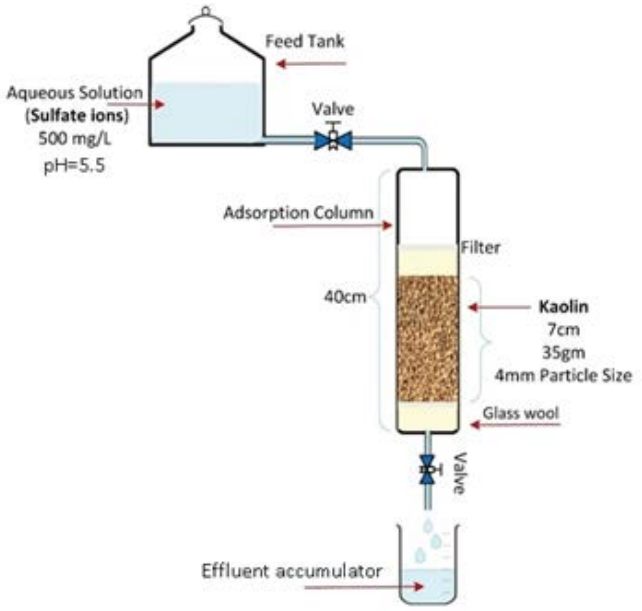

Fig. 1. Schematic diagram of the experimental setup.

of adsorbent during the experiment. The kaolin bed was packed into the column and wetted with ultrapure water. The average particle size studied was 4 mm. The solution was allowed to flow through the bed downwards from the reservoir by gravity at a constant flow rate by using a manually controlled valve fixed at the exit of the feed tank. The feed's flow rate through the bed was measured by collecting a known volume of water for a specific time. Three different flow rates were studied (6.6, 12, and 24 mL/min). The residual sulfate ions concentration in the effluent stream was analyzed using a spectrophotometer (UV-visible), model UV-Vis spectrophotometer UV-1800 – Shimadzu. The measurements were carried out at a maximum wavelength (λ_{max}) of 420 nm. Column studies were completed when the column attained exhaustion.

3. Results and discussions

3.1. Kaolin adsorbent characteristics

A mineralogical investigation of the raw kaolin was carried out using X-ray fluorescence (XRF) analysis. The chemical composition is presented in Table 1. The elements determined in kaolin clay have been expressed as oxides in the whole sample, as shown in Table 1. Results indicated that the raw kaolin deposits are majorly composed of kaolinite, quartz, and hematite. According to the XRF chemical analysis, the used kaolin as adsorbent composed mainly of 67.35 wt% of silica and 8.62 wt% of alumina. Obviously, the presence of a large amount of hematite of about 17.48 wt% is higher than alumina. The nature of the sulfate bond to iron oxides (hematite) as sulfate ion bond is known and was evaluated as a strong bond [31]. Moreover, oxide surfaces generally are considered a very powerful adsorbent for sulfate ions. The composition of kaolin candidates it as a suitable and powerful adsorbent for sulfate ions due to large areas of oxide surfaces that can

Table 1
Chemical composition (XRF) (wt%) of the raw kaolin clay samples used in this study

Al_2O_3	8.62
CaO	0.65
Fe_2O_3	17.48
K_2O	0.27
MgO	0.22
SO_3	0.14
SiO_2	67.35
Loss of ignition	5.27

bond with sulfate ions. On the other hand, the modification of the surface of kaolin by the adsorption of $BaCl_2$ will enhance the sulfate removal due to the bonding between $BaCl_2$ and sulfate ions according to the reaction:

$$BaCl_{2(aq)} + SO^{-2}_{4(aq)} \rightarrow Cl^{-}_{(aq)} + BaSO_{4(s)} \quad (1)$$

3.2. FTIR analysis

FTIR spectra of raw kaolin and modified kaolin are presented in Fig. 2. The corresponding functional groups of raw kaolinite. Both raw kaolin and modified kaolin demonstrated 3,691.89 and 3,619.5 cm^{-1} corresponds to the inner hydroxyl groups, located between octahedral and tetrahedral sheets [32,33]. The bands for raw kaolin at 1,032.7, 1,003.78 and modified kaolin with a significant shifting at 1,075.5 and 1,004.78 cm^{-1} were attributable to Si–O stretching vibration.

The band at 913.76 and 911.2 cm^{-1} was assigned to Si–OH or Al–Al–OH vibration [34]. The peaks at 777.3 and 789.3 cm^{-1} were attributed to Si–O–Al stretching vibration, respectively [33,34]. A weak absorption band at 691.5 and 696.2 cm^{-1} was attributed to Si–O–Si bending vibration [34].

Vibration at 438 and 429.8 cm^{-1} for both raw and modified kaolin can be related to the deformation mode of Si–O or Al–O bonds [35]. For the modified kaolin, a significant band was observed at 410.63 corresponds to Ba–Cl in-plane bending [36].

It can be concluded that the sorption of $BaCl_2$ on kaolin showed no change in the basic structure of kaolin, and this allows us to say that adsorption is done by physical interaction forces mainly shown at 410.63 cm^{-1} [36]. Hence, the maximum intensities have decreased slightly, and the adsorption bands' position shifted significantly; this may be related to an energy variation due to the bonds established and probably justifies the feasibility of adsorption [37].

3.3. Fixed-bed column breakthrough curves

Fig. 3 presents the experimentally measured breakthrough behavior of the continuous column adsorption process of sulfate ions on kaolin at different flow rates. All the other parameters are kept constant (bed height = 7 cm; pH = 5.5; inlet concentration C_1 = 500 mg/L; mass of adsorbent = 35 g).

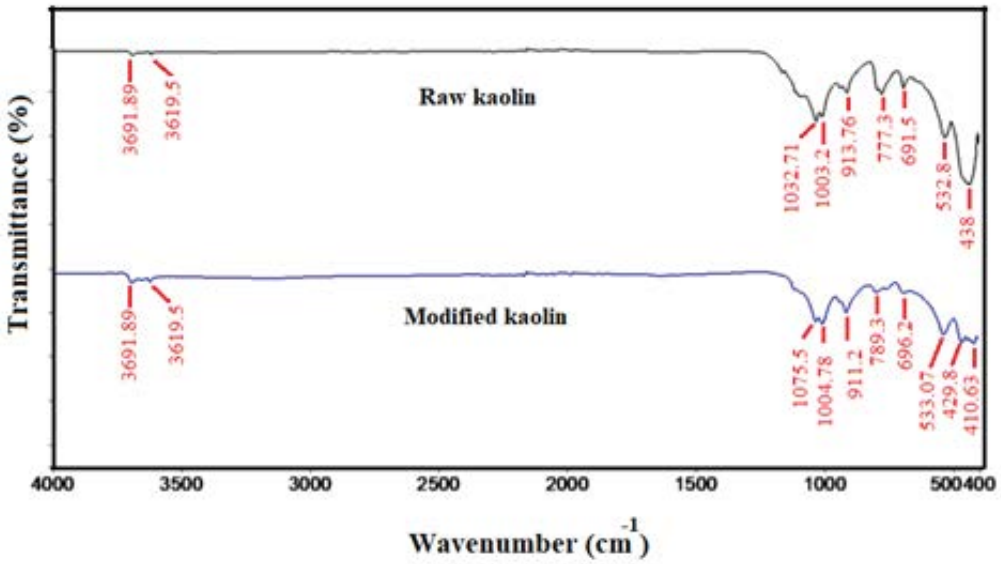

Fig. 2. FTIR spectra of raw kaolin and modified kaolin.

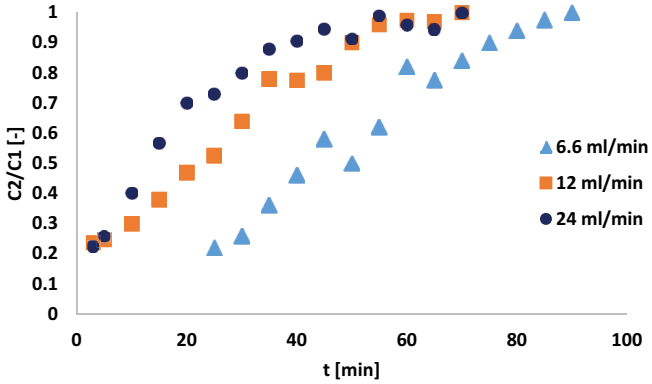

Fig. 3. The experimentally measured breakthrough at different flow rates.

In a fixed bed column, the flow of contaminated water forms a front moving downwards through the bed. The front separates the saturated (exhausted) part of the bed and the adsorption mass transfer zone where the adsorption process takes place. As the kaolin adsorbent becomes exhausted over time, the mass transfer zone decreases and moves downwards across the bed leaving behind the portion of the adsorbent bed that is saturated by the contaminants which increases over time. Consequently, the front of the mass transfer zone reaches the end of the column and breakthrough occurs. The breakthrough point is typically known as the point when the ratio of C_2/C_1 becomes between 0.1 and 0.9.

In this study the time to reach a value of $C_2/C_1 = 0.5$ ($t_{0.5}$) is focused due to its importance as a significant process design parameter [38,39]. At $t_{0.5}$ the adsorbent is regularly changed in the case of industrial scale application, that is, at 50% breakthrough of the bed. However, after the 50% breakthrough point, the column can still operate until the ratio C_2/C_1 becomes 0.90. This point is termed as $t_{0.9}$ where the column will be practically exhausted.

The extent of adsorption for the continuous operation depends on the flow rate of the aqueous solution. The breakthrough and exhaust times are considered essential values in the adsorption fixed-bed column's design and operation, and obviously, they are strongly dependent on the flow rate. Fig. 4 displays the dependence of both 50% breakthrough and exhaust times on flow rate.

Fig. 4 shows that the time taken to achieve 50% breakthrough and the exhaust time decreases with increased flow rate; it is obvious that the adsorption efficiency is higher at lower flow rates. As the flow rate increased, the contact time between sulfate ions and the surface of modified kaolin adsorbent reduced and thus sulfate ions will pass through the column faster, causing a reduced breakthrough and exhaustion times. Lower flow rates leads to higher residence time of the solution in the column, and the sulfate ions will have more time to diffuse into the pores of kaolin through intra-particle diffusion [40,41]. In other words, the sulfate contained solution leaves the column before equilibrium occurs, causing a reduction in adsorption capacity and service time of the bed. This trend similar to the other research work found in the literature [42].

3.4. Modeling of fixed-bed breakthrough curves

3.4.1. Bohart–Adams model

Bohart–Adams model is a commonly used mathematical model for designing fixed-bed adsorption columns [43,44]. It assumes that the adsorption process follows a rectangular isotherm, and the rate of adsorption is proportional to the adsorbent's capacity and the adsorbate concentration. A simple known linear form of Bohart–Adams model is given by the relation [45–48].

$$\ln\left(\frac{C_2}{C_1}\right) = K_{AB}C_1 t - \frac{K_{AB}N_0 H}{V_0} \quad (2)$$

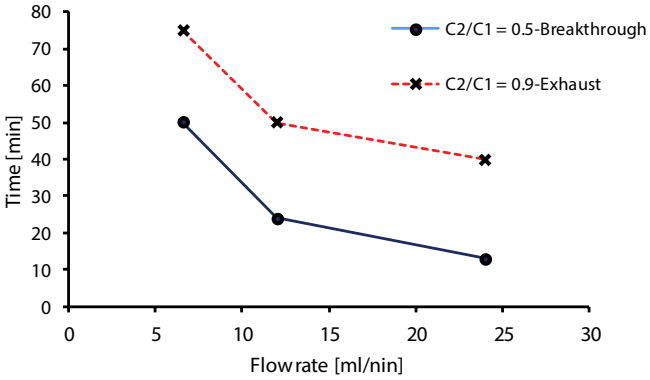

Fig. 4. The measured 50% breakthrough and 90% exhaust times of the bed at the studied flow rates.

where C_1 is the inlet concentration (mg/L), C_2 is the effluent concentration (mg/L), K_{AB} is the Bohart–Adams kinetic constant (L/mg min), V_0 is the linear velocity (flow rate/column section area, cm/min), H is the bed height (cm) and N_0 is the adsorption capacity of the adsorbent per volume of the bed (mg/L). The linear fit of the experimental breakthrough curves according to Bohart–Adams model is shown in Fig. 5, and the estimated Bohart–Adams model parameters K_{AB} and N_0 at the different flow rates are listed in Table 2.

The change of the values of the parameters in Table 2 resulted from the variation of the flow rate of the solution as all the operating conditions (particle size, sorbate inlet concentration, bed height, and pH) were fixed.

From the results presented in Table 2, the values of N_0 which represents the bed capacity per unit volume is higher at higher flow rates. The change in the values of K_{AB} with flow rate is minor and can be neglected. The value of K_{AB} usually changes with variations in parameters that boost the external mass transfer rate. The minor change in K_{AB} values indicated that flow rate plays a minor role in enhancing the external mass transfer rate. This is attributed to the high concentration of sulfate ions (500 mg/L), which govern the external mass transfer.

The range of linear regression R^2 of the Bohart–Adams model lies from 0.73 to 0.92 at the different flow rates, which exhibits a relatively poor fit of the measured breakthrough curves to the Bohart–Adams model. The calculated breakthrough curves from Bohart–Adams model compared to the experimentally measured data are depicted in Fig. 7.

As shown in Fig. 7, the Bohart–Adams model poorly fits the experimental data, however it smooths the experimental breakthrough curve at lower flow rates more precisely than at higher flow rates.

3.4.2. Thomas model

Thomas model is widely applied to model the breakthrough curves and describe the fixed bed adsorption column's performance. Moreover, it estimates the adsorption capacity per one gram of the adsorbent, which is very important in designing a continuous fixed-bed adsorption column.

Thomas model assumes adsorption with Langmuir isotherm with no axial dispersion. The model was derived

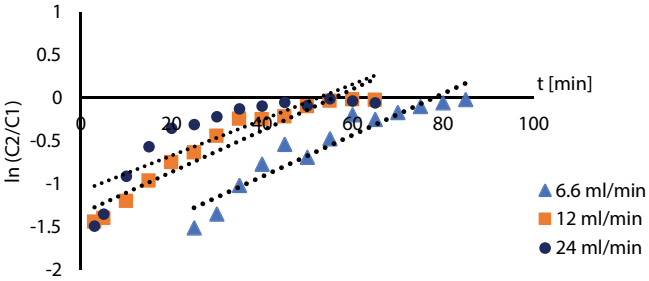

Fig. 5. The linear plot of the experimental breakthrough data according to Bohart–Adams model [Eq. (1)].

Table 2
Estimated Bohart–Adams model parameters at different flow rates

Flow rate, (mL/min)	K_{AB}, (L/mg min)	N_0, (mg/L)	R^2, (–)
6.6	4.82×10^{-5}	19,160.96	0.90
12	4.82×10^{-5}	24,899.97	0.92
24	4.14×10^{-5}	46,838.34	0.73

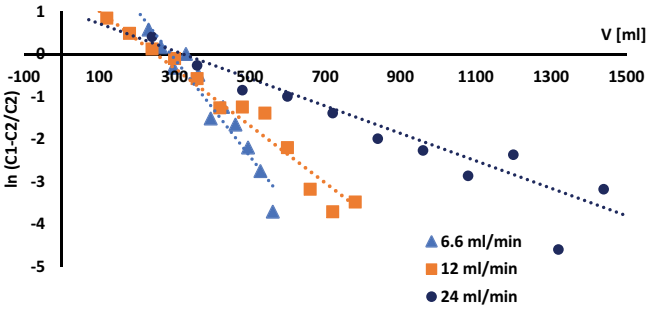

Fig. 6. A plot of the measured breakthrough curves according to the Thomas model.

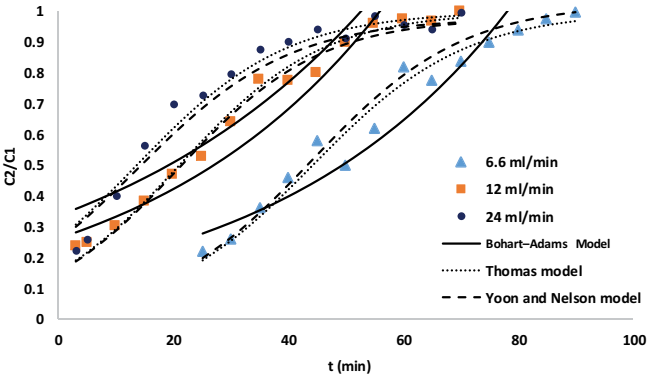

Fig. 7. Experimental and calculated breakthrough curves from Bohart–Adams model, Thomas model and Yoon–Nelson model at different flow rates.

because the rate driving force follows second-order reaction kinetics [47,49–51]. Theoretically, it is suitable to estimate the adsorption process where the external and internal resistances to diffusion is very small [52]. The following relation can express the linearized form of the Thomas model:

$$\ln\left(\frac{C_1 - C_2}{C_2}\right) = -\frac{C_0 K_T}{F} V + \frac{MqK_T}{F} \quad (3)$$

where F is the volumetric feed flow rate (mL/min), K_T is Thomas rate constant (L/min mg), V is the volume of effluent wastewater (mL), q is the maximum adsorption capacity (mg/g). M is the adsorbent mass in the column (g).

The Thomas model parameters (K_T and q) can be estimated from the slope and intercept of the linear plot of $\ln\left(\frac{C_1 - C_2}{C_2}\right)$ against V, which is depicted in Fig. 6. The Thomas model parameters are listed in Table 3.

The results presented in Table 3 indicate a good fit of the experimental breakthrough data to the Thomas model with the R^2 values ranging from 0.88 to 0.96. The results given in Table 2 show that the adsorbent capacity has the highest value at a higher flow rate (24 mL/min). This is in good agreement with the result obtained from Bohart–Adams model (Table 3).

The predicted breakthrough curves from Thomas model equation compared to the experimentally measured data are depicted in Fig. 7. It is obvious that Thomas model provides an excellent fit to the experimental results. Moreover, the fixed-bed column experimental results are fitted more accurately by Thomas model than Bohart–Adams model which exhibits a poor fitting of the experimental breakthrough curves.

3.4.3. Yoon–Nelson model

The Yoon–Nelson model assumes that the decrease in the rate of adsorption probability is directly proportional to the probability of molecule adsorption and the probability of molecule breakthrough. The Yoon–Nelson expression in its linear form is [53]:

$$\ln\left(\frac{C_2}{C_1 - C_2}\right) = K_{YN} t - \tau K_{YN} \quad (4)$$

Table 3
Parameters of Thomas model using linear regression analysis of the experimental breakthrough curves

Flow rate, (mL/min)	K_T, (L/min mg)	q, (mg/g)	R^2, (–)
6.6	1.50×10^{-4}	41.65	0.96
12	1.61×10^{-4}	35.94	0.97
24	1.54×10^{-4}	46.51	0.88

Table 4
Parameters of Yoon–Nelson model using linear fitting of the experimental breakthrough curves

Flow rate, (mL/min)	K_{YN}, (min^{-1})	τ, (min)	R^2, (–)
6.6	7.56×10^{-2}	43.96	0.957
12	8.07×10^{-2}	20.89	0.969
24	7.74×10^{-2}	13.46	0.879

where K_{YN} the Yoon–Nelson is rate constant (min^{-1}) and τ is the time needed to reach 50% of C_1 (min). The value of K_{YN} depends on the column operating conditions such as initial adsorbate concentration, bed height, and feed flow. The values of K_{YN} and τ are estimated from the slopes and intercepts of the linear plot of $\ln\left(\frac{C_2}{C_1 - C_2}\right)$ against t (Fig. 8) at the studied flow rates. The estimated Yoon–Nelson model parameters at the different flow rates are given in Table 4.

It is noticeable that at the flow rates 6.6, 12, and 24 mL/min, the estimated values of τ are 43.9, 20.8, and 13.4 min, respectively. These values are in excellent agreement with the experimental values given in Fig. 4

It can be concluded that at a higher flow rate, the time required for 50% exhaustion of column (τ) is reduced dramatically. This is attributed to the fact that at a higher flow rate, the column is exhausted earlier and the fixed bed is saturated quickly. Moreover, for the higher flow rate the front of the mass transfer zone reached near to the exit of the column more quickly. The value of (τ) is an important design and operation parameter in the case of the fixed-bed column adsorption process. At τ the adsorbent is required to be recurrently changed in the case of industrial scale application.

The higher R^2 linear correlation coefficients given in Table 4 point toward the fact that the experimental data agree with Yoon and Nelson model. Fig. 7 depicts an examination of Yoon and Nelson's fitting model to the measured experimental breakthrough curves. It can be envisaged that the theoretical curves calculated by the Yoon and Nelson model fit very well the measured experimental curves. It is also clear that the Yoon and Nelson model fits the experimental data to a higher degree than the Bohart–Adams model (Fig. 7).

4. Conclusion

In this work, modified kaolin has been considered a low-cost adsorbent to treat wastewater streams polluted with a high concentration of sulfate ions. This adsorbent's benefit is its potential to adsorb sulfate ions with a high adsorption capacity in continuous industrial operations. The continuous adsorption column process is examined at different flow rates and the results indicated that this process exhibits an outstanding performance with a high separation efficiency. This study showed that the modified

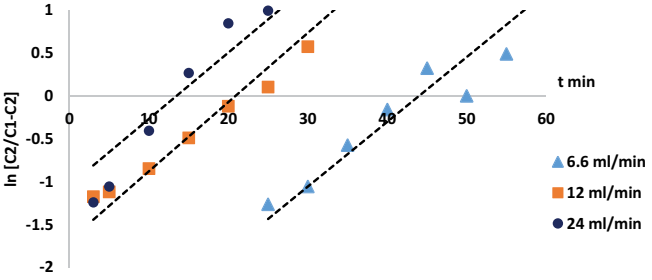

Fig. 8. A plot of the measured breakthrough curves according to the Yoon–Nelson model.

kaolin could be used as a potential adsorbent in continuous packed bed operation for the treatment processes of wastewater contaminated with high sulfate ion concentration. Based on the result obtained, the high removal efficiency of sulfate ion from aqueous solutions by adsorption encourages further research to apply the removal of sulfate ions from brackish water or seawater as a pretreatment step to reduce the fouling of sulfate scaling compounds in thermal and membrane water desalination processes.

References

[1] J. Schleich, T. Hillenbrand, Determinants of residential water demand in Germany, Ecol. Econ., 68 (2009) 1756–1769.

[2] T.M. Al-Momani, "Mohammed-Ezz-Aldien" Ibrahim Dwairi, Physical and technical characteristics of jarash clay deposits from Northern Jordan, Jordan J. Earth Environ. Sci., 9 (2018) 81–88.

[3] PRB, World Population Data Sheet, Demographic Data and Estimates for the Countries and Regions of the World, 1998.

[4] A. Porowski, D. Porowska, S. Halas, Identification of sulfate sources and biogeochemical processes in an aquifer affected by peatland: insights from monitoring the isotopic composition of groundwater sulfate in Kampinos National Park, Poland, Water, 11 (2019) 1388, doi: 10.3390/w11071388.

[5] A. Jiries, T. El-Hasan, M. Al-Hweiti, K.-P. Seiler, Evaluation of the effluent water quality produced at phosphate mines in Central Jordan, Mine Water Environ., 23 (2004) 133–137.

[6] H.S. Al-Zoubi, S.S. Al-Thyabat, Treatment of a Jordanian phosphate mine wastewater by hybrid dissolved air flotation and nanofiltration, Mine Water Environ., 31 (2012) 214–224.

[7] W. Cao, Z. Dang, X.-Q. Zhou, X.-Y. Yi, P.-X. Wu, N.-W. Zhu, G.-N. Lu, Removal of sulphate from aqueous solution using modified rice straw: preparation, characterization and adsorption performance, Carbohydr. Polym., 85 (2011) 571–577.

[8] I. Pikaar, K.R. Sharma, S.H. Hu, W.G. Gernjak, J. Keller, Z. Yuan, Water engineering. Reducing sewer corrosion through integrated urban water management, Science, 345 (2014) 812–814.

[9] H. Sun, B. Shi, F. Yang, D. Wang, Effects of sulfate on heavy metal release from iron corrosion scales in drinking water distribution system, Water Res., 114 (2017) 69–77.

[10] D. Baldwin, A. Mitchell, Impact of sulfate pollution on anaerobic biogeochemical cycles in a wetland sediment, Water Res., 46 (2011) 965–974.

[11] A.M. Silva, R.M.F. Lima, V.A. Leão, Mine water treatment with limestone for sulfate removal, J. Hazard. Mater., 221–222 (2012) 45–55.

[12] WHO, Guidelines for Drinking Water Quality, World Health Organization, 2017. Available at: https://www.who.int/publications/i/item/9789241549950, accessed on.04-04-2021.

[13] Ministry of Water and Irrigation, Jordan "Water-Natural Water", 2009. Available at: http://www.jsmo.gov.jo/en/EServices/Standards/Pages/StdLists.aspx?ics=1306020, accessed on 03-04-2021.

[14] H. Al-Zoubi, N. Hilal, N.A. Darwish, A.W. Mohammad, Rejection and modelling of sulphate and potassium salts by nanofiltration membranes: neural network and Spiegler–Kedem model, Desalination, 206 (2007) 42–60.

[15] H.I. Shaban, A.M. Akbar, M.A. Fahim, Treatment of ammonium sulfate effluents by reverse osmosis, Environ. Sci. Eng., 13 (1978) 315–324.

[16] İ. Can, Ö. Bıçak, S. Özçelik, N. Can, Z. Ekmekçi, Sulphate removal from flotation process water using ion-exchange resin column system, Minerals, 10 (2020) 655–671.

[17] R. Nilsson, Removal of metals by chemical treatment of municipal waste water, Water Res., 5 (1971) 51–60.

[18] R.J. Bowell, A Review of Sulfate Removal Options for Mine Waters, A.P. Jarvis, B.A. Dudgeon, P.L. Younger, Eds., Mine Water 2004 – Proceedings International Mine Water Association Symposium 2, University of Newcastle, Newcastle upon Tyne, 2004, pp. 75–91.

[19] W. Omar, H. Al-Itawi, Removal of Pb^{+2} ions from aqueous solutions by adsorption on kaolinite clay, Am. J. Appl. Sci., 4 (2007) 502–507.

[20] H. Al-Zoubi, M. Zubair, M.S. Manzar, A.A. Manda, N.I. Blaisi, A. Qureshi, A. Matan, Comparative adsorption of anionic dyes (Eriochrome Black T and Congo Red) onto Jojoba residues: isotherm, kinetics and thermodynamic studies, Arabian J. Sci. Eng., 45 (2020) 7275–7287.

[21] P. Taylor, T. Mahmood, A. Khan, A. Naeem, M. Hamayun, M. Muska, Adsorption of Ni(II) ions from aqueous solution onto a fungus *Pleurotus ostreatus*, Desal. Water Treat., 57 (2015) 7209–7218.

[22] W. Omar, R. Al Dwairi, Z.S. Abu-Hamatteh, N. Jabarin, Investigation of natural Jordanian zeolite tuff (JZT) as adsorbent for TOC removal from industrial wastewater in a continuous fixed bed column: study of the influence of particle size, Desal. Water Treat., 152 (2019) 26–32.

[23] Y. Rajesh, G. Namrata, U. Ramgopal, Ni(II) adsorption characteristics of commercial activated carbon from synthetic electroless plating solutions, Desal. Water Treat., 57 (2016) 13807–13817.

[24] W. Stigliani, Changes in valued capacities of soils and sediments as indicators of nonlinear and time-delayed environmental effects, Environ. Monit. Assess., 10 (1988) 245–307.

[25] M. Matłok, R. Petrus, J.K. Warchoł, Equilibrium study of heavy metals adsorption on kaolin, Ind. Eng. Chem. Res., 54 (2015) 6975–6984.

[26] A. Sdiri, T. Higashi, T. Hatta, F. Jamoussi, N. Tase, Evaluating the adsorptive capacity of montmorillonitic and calcareous clays on the removal of several heavy metals in aqueous systems, Chem. Eng. J., 172 (2011) 37–46.

[27] W. Gao, S. Zhao, H. Wu, W. Deligeer, S. Asuha, Direct acid activation of kaolinite and its effects on the adsorption of methylene blue, Appl. Clay Sci., 126 (2016) 98–106.

[28] R. Frost, E. Mako, J. Kristóf, E. Horvath, T. Kloprogge, Mechanochemical treatment of kaolinite, J. Colloid Interface Sci., 239 (2001) 458–466.

[29] A. Emam, L. Ismail, M. Abdelkhalek, Azzarehan, Adsorption study of some heavy metal ions on modified kaolinite clay, Int. J. Adv. Eng. Technol. Manage. Appl., 3 (2016) 152–163.

[30] G. Atun, E. Bascetin, Adsorption of barium on kaolinite, illite and montmorillonite at various ionic strengths, Radiochim. Acta, 91 (2003) 223–228.

[31] H. Watanabe, C.D. Gutleben, J. Seto, Sulfate ions on the surface of maghemite and hematite, Solid State Ionics, 69 (1994) 29–35.

[32] A.K. Panda, B.G. Mishra, D.K. Mishra, R.K. Singh, Effect of sulphuric acid treatment on the physico-chemical characteristics of kaolin clay, Colloids Surf., A, 363 (2010) 98–104.

[33] C. Belver, M.A. Bañares Muñoz, M.A. Vicente, Chemical activation of a kaolinite under acid and alkaline conditions, Chem. Mater., 14 (2002) 2033–2043.

[34] J.-B. Chai, P.-I. Au, N.M. Mubarak, M. Khalid, W.P.-Q. Ng, P. Jagadish, R. Walvekar, E.C. Abdullah., Adsorption of heavy metal from industrial wastewater onto low-cost Malaysian kaolin clay-based adsorbent, Environ. Sci. Pollut. Res., 27 (2020) 13949–13962.

[35] N. Caponi, G. Collazzo, S.L. Jahn, G. Dotto, M. Mazutti, E. Foletto, Use of Brazilian kaolin as a potential low-cost adsorbent for the removal of malachite green from colored effluents, Mater. Res., 20 (2017) 14–22.

[36] E. Peter, A. Dabulo, G. Thillainayagam, Growth and characterization of barium chloride dihydrate crystal, Int J. Sci. Res., 8 (2019) 1775–1779.

[37] G. El Mouhri, M. Merzouki, H. Belhassan, Y. Miyah, H. Amakdouf, R. Elmountassir, A. Lahrichi, Continuous adsorption modeling and fixed bed column studies: adsorption of tannery wastewater pollutants using Beach Sand, J. Chem., 2020 (2020) 1–9.

[38] Y. Han, S. Shunan, F. Yang, Y. Xie, M. Zhao, J.-R. Li, Size-exclusive and coordination-induced selective dye adsorption

in a nanotubular metal–organic framework, J. Mater. Chem. A, 3 (2015) 12804–12809.
[39] E.I. Unuabonah, M.I. El-Khaiary, B.I. Olu-Owolabi, K.O. Adebowale, Predicting the dynamics and performance of a polymer–clay based composite in a fixed bed system for the removal of lead(II) ion, Chem. Eng. Res. Des., 90 (2012) 1105–1115.
[40] S. Kundu, A.K. Gupta, As(III) removal from aqueous medium in fixed bed using iron oxide-coated cement (IOCC): experimental and modeling studies, Chem. Eng. J., 129 (2007) 123–131.
[41] K.S. Rao, S. Anand, P. Venkateswarlu, Modeling the kinetics of Cd(II) adsorption on *Syzygium cumini* L leaf powder in a fixed bed mini column, J. Ind. Eng. Chem., 17 (2011) 174–181.
[42] R. Han, Y. Wang, X. Zhao, Y. Wang, F. Xie, J. Cheng, M. Tang, Adsorption of methylene blue by phoenix tree leaf powder in a fixed-bed column: experiments and prediction of breakthrough curves, Desalination, 245 (2009) 284–297.
[43] K. Chu, Fixed bed sorption: setting the record straight on the Bohart–Adams and Thomas models, J. Hazard. Mater., 177 (2010) 1006–1012.
[44] D.O. Cooney, Adsorption Design for Wastewater Treatment, Taylor & Francis, 1998.
[45] G.S. Bohart, E.Q. Adams, Some aspects of the behavior of charcoal with respect to chlorine, J. Am. Chem. Soc., 42 (1920) 523–544.
[46] Z. Chowdhury, S.B. Abd Hamid, S. Zain, Evaluating design parameters for breakthrough curve analysis and kinetics of fixed bed columns for Cu(II) cations using lignocellulosic wastes, BioResources, 10 (2014) 732–749.
[47] Z. Aksu, F. Gönen, Biosorption of phenol by immobilized activated sludge in a continuous packed bed: prediction of breakthrough curves, Process Biochem., 39 (2004) 599–613.
[48] K.H. Chu, Breakthrough curve analysis by simplistic models of fixed bed adsorption: in defense of the century-old Bohart–Adams model, Chem. Eng. J., 380 (2020) 122513–122521.
[49] H.C. Thomas, Heterogeneous ion exchange in a flowing system, J. Am. Chem. Soc., 66 (1944) 1664–1666.
[50] J. Wu, H.-Q. Yu, Biosorption of 2,4-dichlorophenol by immobilized white-rot fungus *Phanerochaete chrysosporium* from aqueous solutions, Bioresour. Technol., 98 (2007) 253–259.
[51] S. Ayoob, A. Gupta, P. Bhakat, Analysis of breakthrough developments and modeling of fixed bed adsorption system for As(V) removal from water by modified calcined bauxite (MCB), Sep. Purif. Technol., 52 (2007) 430–438.
[52] Z. Xu, J. Cai, B. Pan, Mathematically modeling fixed-bed adsorption in aqueous systems, J. Zhejiang Univ. Sci. A, 14 (2013) 155–176.
[53] Y.H. Yoon, J.H. Nelson, Application of gas adsorption kinetics. I. A theoretical model for respirator cartridge service life, Am. Ind. Hyg. Assoc. J., 45 (1984) 509–516.